THE JOURNAL OF PHYSICAL CHEMISTRY C

ARTICLE

pubs.acs.org/JPCC

Carboxylic Acid-Directed Clustering and Dispersion of ZrO_2 Nanoparticles in Organic Solvents: A Study by Small-Angle X-ray/Neutron Scattering and NMR

Sho-Hsun Wang,[†] Ya-Sen Sun,*[,†] Anthony Shiaw-Tseh Chiang,[†] Hui-Fang Hung,[†] Ming-Chou Chen,[‡] and Kathleen Wood[§]

[†]Department of Chemical and Materials Engineering, National Central University, Taoyuan 32001, Taiwan

[‡]Department of Chemistry, National Central University, Taoyuan 32001, Taiwan

[§]Bragg Institute, Australian Nuclear Science and Technology Organisation, Locked Bag 2001, Kirrawee DC NSW 2232, Australia

Supporting Information

ABSTRACT: The stable dispersion of nanoparticles in organic solvents, essential for their practical application, is often achieved by the grafting of organic dispersants. Good dispersion is usually assumed when a transparent colloidal sol is formed. However, even in such a case, the dispersion may not be in the form of distinct nanoparticles. In this study, zirconia nanoparticles have been modified with a series of carboxylic acids so that they can be dispersed in polar protic/aprotic solvents or nonpolar organic solvents as transparent colloidal sols. The dispersed state in these solvents was characterized by SAXS and SANS. In most cases, the transparent sol consists of "soft" secondary clusters generated from the ZrO_2 nanoparticles. The size and fractal structure of the dispersed clusters varied with the acid modifier. Only in the linoleic acid-modified case and with chloroform as the solvent was the ZrO_2 dispersed as primary particles. However, the same modification leads to secondary clusters in other solvents, such as toluene and benzene, with similar solubility parameters. The difference in the dispersion states calls for a molecular-level interpretation. It was proposed that the grafted LOA exists as a swollen and extended brush in benzene and toluene, but as a folded and compact shell in chloroform. The proposed shell structures were then confirmed by the proximity of the chain tail with the middle section observed on 2D NOESY ^{1}H NMR spectra.

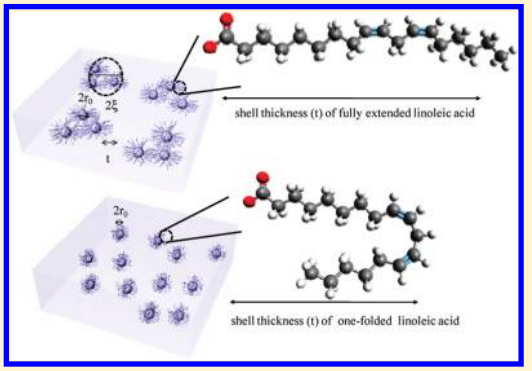

INTRODUCTION

The incorporation of inorganic nanoparticles is one of the effective ways to modulate the refractive index of an optical polymer. Among the possible nanofillers, ZrO_2 is preferred for its high transparency in both the UV and the visible ranges. Nanocomposites of ZrO_2 nanoparticles with a variety of acrylate photopolymers have been studied as materials for holographic recording,[1−3] LED encapsulation,[4] and other optical functional materials[5−7] or coatings.[8−10]

ZrO_2 nanoparticles can be prepared by many different processes. For the preparation of optical nanocomposites, the particle size must be much smaller than 10 nm so that excessive Rayleigh scattering is avoided. Furthermore, the hydrophilic surface of ZrO_2 must be modified to be compatible with organics, thus intimately mixed with the polymer. Many different capping agents have been employed for such a purpose. Among them, the silane coupling agents are most popular, particularly the one with a methacrylic group. Carboxylic acids are also favored for not introducing unnecessary siloxane bridges.

After surface modification, the nanoparticles are usually dispersed in a solvent before mixing with the desired monomers or oligomers. For optical applications where transparency is critical, a uniform distribution of the nanoparticles in the organic phase is essential. Thus, it is important to keep the nanoparticles from aggregating into a larger size. However, it is known that nanoparticles, even after surface modification, seldom disperse in solvent as primary units. The competition and balance between short-range attraction and long-range repulsion may yield a variety of anisotropic superstructures (clusters or aggregates).[11,12] The mixture of nanoparticles and oligomers in solvent might still be transparent as long as the size and refractive index of the composite clusters or aggregates are below the scattering limit, but the rheology[13−15] of the mixed compositions and the mechanical properties[16] of the final nanocomposite will be greatly influenced by the shape, size, structure, and distribution of the clusters.

Dynamic light scattering (DLS) and transmission electron microscopy (TEM) had been the main tools to study the dispersion

Received: March 9, 2011
Revised: May 5, 2011
Published: May 25, 2011

of surface-modified nanoparticles in solvents.[17−20] However, DLS gives only the cluster size, but not its structure. TEM analysis is made on dried samples, and is strongly affected by the sample preparation procedures. Comparing to the above tools, small-angle X-ray and neutron scattering can be done in situ and give more information concerning the nanometer-scale structure of the dispersed phase.

In this work, the dispersion behavior of carboxylic acid-modified zirconia nanoparticles in various protic/aprotic and nonpolar organic solvents is studied by both small-angle X-ray scattering (SAXS) and small-angle neutron scattering (SANS). The nanoparticles were dispersed as primary units in only a single combination of modifier (linoleic acid) and solvent (chloroform). In all other cases, the modified particle formed "soft" secondary clusters whose size and fractal structure varied with the acid modifier. The peculiar behavior of linoleic acid was attributed to the conformation of the organic shell in chloroform. This proposal was further substantiated using ^{1}H NMR.

EXPERIMENTAL SECTION

Materials. Redispersible ZrO_2 nanocrystals were produced from the low-temperature (110 °C) hydrothermal reaction of zirconium hydroxide nanoparticles produced by hydrolysis at a fixed pH value.[21] Briefly, 64.4 g of $ZrOCl_2 \cdot 8H_2O$ was dissolved in 58 g of DI water, to which 2.1 g of methacrylic acid was added. The mixture was stirred for 30 min at RT to dissolve the $ZrOCl_2$ until a pale green transparent solution resulted. The MA added to the $ZrOCl_2 \cdot 8H_2O$ solution was to protect the zirconium polycation and to block the formation of large clusters.

The zirconium precursor was then heated at 110 °C for 24 h before being hydrolyzed in a buffer solution with 4 M NaOH. The buffer solution consists of 10 g of NH_4HCO_3 and 5.5 g of triethanolamine (TEA) in 800 g of DI water. The hydrolysis was done at a fixed pH value of 10 by controlling the addition rates of the acid and base. The buffered mixture remained clear during the whole neutralization process if the neutralization step lasted for more than 4 h. The hydrolysis product was collected by flocculating with acid (HCl) at a pH ∼ 5.4. The excess electrolytes were washed away by repeated centrifugation. IR analysis of the washed precipitates obtained indicated the absence of MA, but the existence of TEA. This was because the hydrolysis was done at pH = 10, which is well above the iso-electric point (IEP) of zirconium hydroxide. The surface of the hydrated hydroxide nanoparticles produced would be negatively charged and repel the MA anion, but attract the TEA cation.

In the final step, the washed hydroxide product was dispersed in water and adjusted to 6 wt % and a pH value of 11.5, then subjected to hydrothermal reaction at 110 °C for 15 h. The reaction product was centrifuged, with the interstitial water replaced by acetone, then vacuum-dried into powders. The powders were redispersible in water, leading to a transparent sol with pH ∼ 10.

A series of carboxylic acids (acetic, acrylic, methacrylic, propionic, butyric, and linoleic) were employed as the surface modifier. The precipitates were collected by centrifugation and vacuum-dried into fluffy powders. The products are denoted as Ac−, AA−, MA−, PA−, BA−, and LOA−ZrO_2 in the same sequence. When modifying the ZrO_2 with carboxylic acid, the pH value must always be kept below the IEP so that chelating is possible (see the Supporting Information, Figure S1). For example, MA modification was conducted by adding these powders into an aqueous MA solution at a pH value of about 4.3−4.6 and stirring at 60 °C for 2 h. The precipitates were centrifuged and repeatedly washed by water and vacuum-dried at 80 °C to obtain modified powders. LOA modification was conducted similarly by adding the powders into an LOA/ethanol solution at pH = 6 and stirring at 60 °C for 2 h. The precipitates were centrifuged and repeatedly washed with ethanol and vacuum-dried at 30 °C to obtain the LOA-modified powders. TGA analysis (Figure S2, Supporting Information) showed that the organic loading was 28, 32, 32, 35, 35, and 50 wt % for Ac−, AA−, PA−, MA−, BA−, and LOA−ZrO_2, respectively.

Table 1. Goodness of Dispersion for Carboxylic Acid-Modified ZrO_2 Nanoparticles in Various Solvents[a]

	acid					
solvent	Ac	PA	AA	BA	MA	LOA
H_2O	o	x	x	x	x	x
EtOH	o	x	x	x	o[b]	x
THF	x	o	o	o	o	x
chloroform	x	o	o	o	o	o
hexane	x	x	x	x	x	o
benzene	x	x	x	o	o	o
toluene	x	x	x	o	o	o
MMA	x	x	x	o	o	x

[a] By visual inspection at a 10 wt % loading of ZrO_2: o, dispersible as transparent sol; x, precipitation or flocculation. [b] Incompletely dried.

The modified powders could be dispersed in various organic solvents as transparent sols. The nanoparticle dispersions were always at 10 wt % in solid, unless otherwise mentioned. The judgment on a good dispersion was made when the dispersion appeared as transparent or slightly bluish translucent. In such a case, the sol remains transparent (translucent) for at least 3 months. The transparency of the sol can of course be defined more clearly by a transmission spectrum, as given by the example in Figure S3 (Supporting Information). The goodness of dispersion, as observed visually, is tabulated in Table 1.

SAXS and SANS. Various sols, with 0.1−1 wt % ZrO_2, were subjected to SAXS measurements. The SAXS experiments were performed at beamline BL23A of the National Synchrotron Radiation Research Center (NSRRC), Hsinchu, Taiwan. The configuration of the SAXS at BL23A was detailed elsewhere.[22] A monochromatized X-ray radiation source with an energy of 12 keV (wavelength, λ = 1.03 Å) was employed, and 2D SAXS patterns were typically collected for 180−300 s with a Mar165 CCD detector (Mar USA Inc., Evanston, IL, USA) with a 512 × 512 pixel array. The sample-to-detector distance was 2520.17 mm. After data reduction with homemade software, profiles of the scattering intensity (I) versus scattering vector, Q ($Q = 4\pi \cdot \sin(\theta/2)/\lambda$, where θ is the scattering angle), were obtained. The calibration of the detector pixels in terms of scattering vector was made with a silver behenate standard, whose Q_{max} was 0.1076 Å^{-1}. To remove the background scattering from solvents, air, and sealed kapton windows, precise measurements on the transmission of ZrO_2 dispersed sols and the corresponding organic solvents were also made. A 1.89 mm thick polyethylene (PE) block was used as the calibration standard, to convert the 1D scattering profiles to absolute intensities after background subtraction. The intensity of the diffraction peak of PE, $I(Q)$ = 36.6 cm^{-1}

at $Q = 0.023$ Å^{-1}, was used as the scaling factor between the measured $I(Q)$ and the absolute $I(Q)$.

A more concentrated dispersion (10 wt % in solvents) was employed in the SANS studies. SANS experiments were carried out at the QUOKKA end-station of the Australian Nuclear Science and Technology Organisation (ANSTO) in Australia. Samples were filtered (0.45 μm membrane) and placed in a homemade demountable 1 mm sample cell sealed by quartz windows. A neutron wavelength of 4.9 Å with a 6% wavelength spread (full width at half-maximum) was used. Two sample-to-detector distances (13 and 2 m) were selected to provide a Q range of 0.06−0.3 Å^{-1}. Longer distances were run for 30 min to record the low Q values, whereas the shorter distances were run for 15 min. To perform background subtraction, the corresponding blank measurements with pure solvents were also made. The 2D SANS data, after subtracting the background, were normalized to a standard plexiglas sample to correct for detector efficiency. The corrected and normalized 2D SANS patterns were subsequently integrated to obtain 1D profiles of absolute intensity. All data reduction steps were performed using the NIST macros in Igor Pro using Quokka specific modifications.[23] The experimental scattering profiles were fitted by the Igor Pro using simulated scattering models developed by S. R. Kline.[24]

NMR. Proton NMR spectra (500.13 MHz) were collected with a Bruker Avance DMX500 spectrometer. The samples include 10 wt % LOA dissolved in deuterated chloroform and benzene, as well as LOA−ZrO_2 dispersions in the same set of solvents. Two-dimensional nuclear Overhauser enhancement spectroscopy (2D NOESY) spectra were recorded with a 700 ms mixing time and a recovery delay of 2 s. 2K data points were collected for 512 increments of 8 scans, using TPPI f_i quadrature detection.

Data Analysis and Model Fitting. SAXS data were analyzed by Guinier fitting, power-law fitting, and Beaucage model fitting.[25] For a colloidal dispersion, the scattering intensity can be approximated in the $Q < 1/R_g$ range as[26]

$$\ln I(Q) = \ln I(0) - (Q^2R_g^2)/3 \quad (1)$$

where R_g is the radius of gyration of primary nanoparticles or clusters. In the high-Q region, the intensity decays as a function of Q with a power of $-D_f$, given by[26]

$$I(Q) = AQ^{-D_f} + B \quad (2)$$

where A is a constant, B is the incoherent background, and D_f the power-law exponent. For SAXS data, the incoherent background is subtle and generally set as zero when doing power-law fitting.

When the cluster size is large and beyond the Guinier domain that SAXS can measure, the Guinier approximation given by eq 1 may be invalid. To calculate the size of clusters in a solvent, the Beaucage model given by[25]

$$I(Q) = G\exp\left(-\frac{Q^2R_g^2}{3}\right) + B\left\{\frac{\left[\operatorname{erf}\left(\frac{QR_g}{\sqrt{6}}\right)\right]^3}{Q}\right\}^P \quad (3)$$

was used, where the first term on the right-hand side represents the Guinier form at low Q and the second term denotes the power-law form at high Q. In here, $G = n^2N_pI_e$ is the exponential prefactor, where n is the number of electrons within a particle, N_p is the number of particles within a scattered volume, and I_e is the scattering factor of an electron. For Porod's law, $B = 2\pi N_p\rho_e^2S_pI_e$, where ρ_e is the number density and S_p is the surface of the particle.[25]

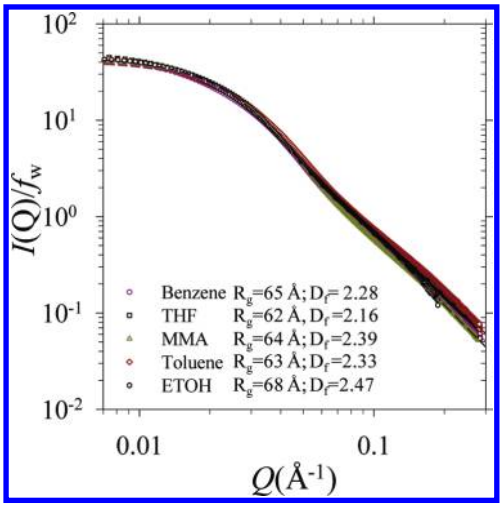

Figure 1. Weight-fraction (f_w)-normalized experimental SAXS profiles (symbols) of MA−ZrO_2 dispersed in various organic solvents. The dashed lines represent the fitted profiles based on the Beaucage model with the parameters listed in the figure.

For the SANS studies, the scattering from the grafted organic materials is not negligible. Thus, the SANS data were analyzed using a core−shell model composed of a polydisperse core with a constant shell thickness. For spheres with a core−shell structure[27]

$$P(Q) = \frac{\text{scale}}{V_t}\left[\frac{3V_c(\rho_c - \rho_s)j_1(Qr_c)}{Qr_c} + \frac{3V_t(\rho_s - \rho_{\text{solvent}})j_1(Qr_t)}{Qr_t}\right] + bkg \quad (4)$$

where $j_1 = (\sin r - r\cos r)/r^2$ is the first-order Bessel function, $r_t = r_c + t_s$ and $V_i = (4\pi/3)r_i^3$ represent the radius and volume, and the subscripts c and s represent the core and shell, respectively. t_s is the thickness of the shell. The Schultz distribution can be incorporated into eq 4 to give a polydispersity in the core radius.[28]

When surface-modified nanoparticles with a polydisperse core−shell structure aggregate into a fractal structure with a fractal dimension D_f and a correlation length ξ, the fractal model can be incorporated into eq 4 to fit the SANS intensity. We have

$$S(Q) = 1 + \frac{\sin[(D_f - 1)\tan^{-1}(Q\xi)]}{(Qr_0)^{D_f}}\frac{D_f\Gamma(D_f - 1)}{\left[1 + \frac{1}{Q^2\xi^2}\right]^{(D_f-1)/2}} \quad (5)$$

where radius r_0 is for the primary nanoparticle that builds the fractal structure.[29]

RESULTS AND DISCUSSION

SAXS Characterization. According to the analysis in our previous paper,[21] the crystalline ZrO_2 nanoparticles produced

dx.doi.org/10.1021/jp202243z |J. Phys. Chem. C 2011, 115, 11941–11950

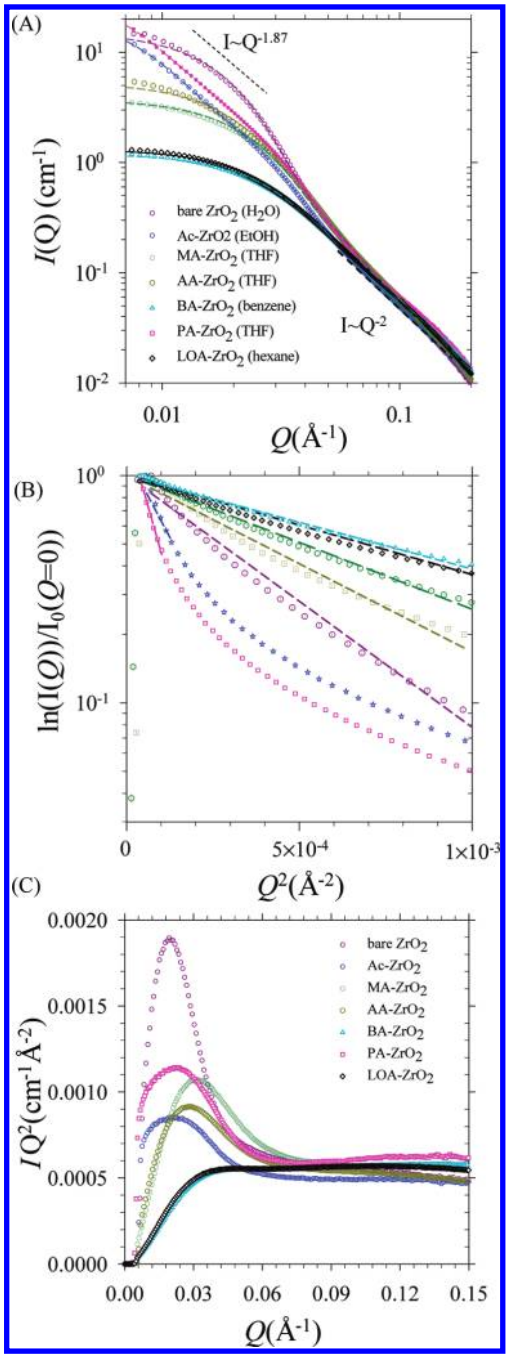

Figure 2. (A) SAXS intensity versus wave vector data for surface-modified ZrO_2 (0.1 wt %) dispersed in different solvents. (B) Guinier plot of the same SAXS data set. (C) Kratky plot (IQ^2 vs Q) of the same SAXS data set.

had a BET surface of 177 m^2/g and a grain size of ~11 nm. The powders were dispersible in water if modified with citric acid and tartaric acid, and in chloroform and hexane when modified with oleic acid. Since then, the preparation procedures have been further improved. Particularly, the washing after hydrothermal crystallization was more thorough and a vacuum-drying step was added after the carboxylic acid modification. Before surface modification by carboxylic acids, the bare ZrO_2 is dispersible (almost transparent at 10 wt %) in water. That modified with various carboxylic acids can be dispersed in polar protic (alcohols), aprotic, and nonpolar organic solvents, as shown in Table 1. The MA−ZrO_2 and BA−ZrO_2 are particularly interesting, because they can be dispersed in most solvents tested, ranging from protic/aprotic to nonpolar ones, as well as methyl methacrylate (MMA) monomer. In contrast, that modified with smaller acids are preferably dispersed in polar protic/aprotic solvents, whereas that with long-chain acids favors the nonpolar organic solvents.

Table 2. Radii of Gyration and the Fractal Dimensions of the Clusters Obtained from Fitting the Data Shown in Figure 2A to the Beaucage Model[a]

modifier	unmodified	Ac−	PA−	AA−	MA−	BA−	LOA−
solvent	H_2O	EtOH	THF	THF	THF	benzene	hexane
R_g (Å)	94	55	44	79	62	54	57
D_f	2.47	2.15	2.17	2.45	2.16	2.34	2.47
R_g* (Å)		213	232				
D_f*		1.88	1.87				

[a] The superscript * represents the size and fractal dimension of the diffusion-limited aggregates grown from the Ac− or PA−ZrO_2 clusters.

Diluted dispersions of MA−ZrO_2 (at 0.1 or 1 wt %) in various solvents were first studied by SAXS. The experimental scattering profiles and the fitted curves based on the Beaucage model are shown together in Figure 1. The experimental data indicate that the structure of the MA−ZrO_2 is independent of the solvent they are dispersed in. The radii of gyration estimated from the curve-fitting were in the range of 62−68 Å, and the fractal dimension D_f ranged from 2.16 to 2.47. Both suggest that the MA−ZrO_2 was dispersed as clusters in these organic solvents.

The structural details of the carboxylic acid-modified ZrO_2 nanoparticles (at 0.1 wt %) were also studied with SAXS. The results are presented in Figure 2A, where data on the aqueous dispersion of unmodified ZrO_2 nanoparticles are also included. The behaviors of the scattering intensity profiles can be divided into two regions. The absolute intensity at low Q varies with the modifier, but merges to a single curve at high Q. The intensity at low Q seems to decrease as the length of the carboxylic acid increases. For the BA−ZrO_2 and the LOA−ZrO_2 cases, the intensity reaches a plateau at the low-Q limit. For the Ac−ZrO_2 and the PA−ZrO_2 cases, the scattering intensity decays with approximately $I \sim Q^{1.78}$. This power-law decay at low Q indicates the development of very large and loose aggregates through the diffusion-limited cluster−cluster aggregation.[30] Because the size of these aggregates is beyond the Guinier domain SAXS can measure, it cannot be estimated by the Guinier approximation. On the other hand, all data except that with acetic acid and propionic acid are linear on the Guinier plots shown in Figure 2B, and their cluster sizes can be estimated by the slope.

For the Ac−ZrO_2 and the PA−ZrO_2 cases, the size of the large aggregates must be estimated by fitting the scattering profile to the Beaucage model (eq 3). The results obtained from fitting were also tabulated in Table 2. For consistency, all other data were also fitted to the same model to extract the corresponding fractal dimensions and the cluster sizes.

According to Table 2, both the Ac−ZrO_2 and the PA−ZrO_2 clusters grew into rather large aggregates, with R_g* ~ 213 Å and D_f = 1.88 for the former and R_g ~ 236 Å and D_f = 1.87 for the latter. The low fractal dimension in both cases indicates that they are rather loosely linked. All other cases in this table were dispersed in the form of individual clusters. The unmodified ZrO_2 has a fractal dimension of D_f = 2.47 and a cluster size of

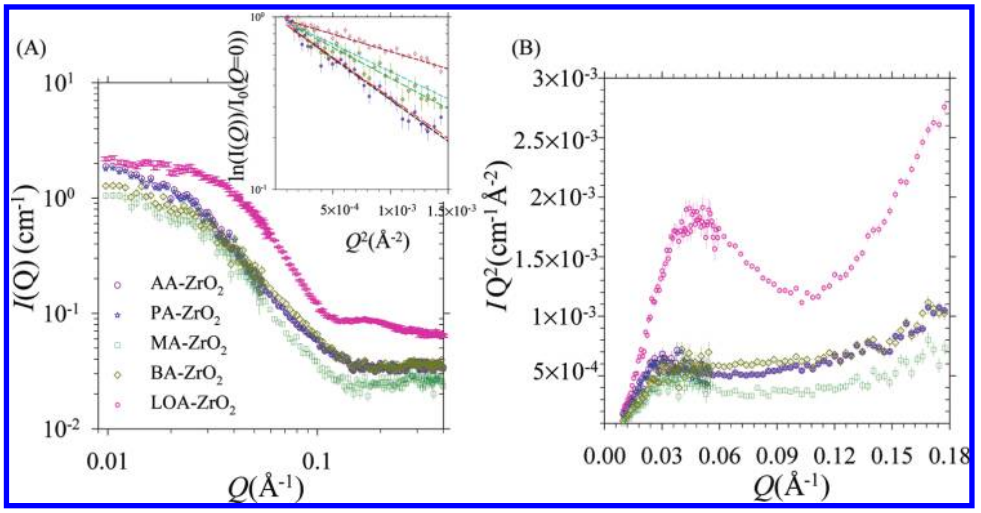

Figure 3. (A) Neutron scattering intensity for carboxylic acid-modified ZrO_2 dispersed in chloroform. The inset shows the Guinier plot. (B) Kratky plot (IQ^2 vs Q) for the same SANS data set.

95 Å. The cluster size reduced to ~60 Å when modified with acids, but the fractal dimension remained at a similar value. The details of these cluster structures are more easily differentiated from the corresponding Kratky plot (IQ^2 versus I) shown in Figure 2C. Here, the unmodified ZrO_2 nanoparticles exhibit a sharp peak at low Q, whereas BA− or LOA−ZrO_2 only leads to a plateau. The former is a typical characteristic of spherical aggregates, whereas the latter resembles the Gaussian soft spheres.[13,31,32] The clusters formed by MA−ZrO_2 should be somewhere in between.

SANS Characterization. As shown in Table 1, all modified nanoparticles except Ac−ZrO_2 can be dispersed in chloroform. Because the X-ray intensity is significantly attenuated by the heavy chlorine element, the chloroform sols are unsuitable for SAXS measurement. Consequently, SANS was used to characterize the structural details of the dispersion in chloroform. Shown in Figure 3A are the obtained data.

In this figure, the intensity falls exponentially according to the Guinier approximation at the low-Q region (0.01−0.03 Å^{-1}). Within this Q range, the scattering feature is provided by the primary nanoparticles or the secondary clusters whose size is within the Guinier range. The Guinier curves gathered in the inset reveal that the radius of gyration for the clusters seems to decrease with increasing length of the acid. However, unlike the SAXS data where the intensity decayed with a power-law at very high Q, the SANS curves reveal a plateau-like feature at the same Q range (0.1−0.4 Å^{-1}). The high-Q plateau is the result of both coherent and incoherent scattering of the grafted carboxylic acids. Particularly, the SANS profile of LOA−ZrO_2 reveals a broad hump around Q = 0.177 Å^{-1}, a signature of a core−shell structure.

Figure 3B shows the corresponding Kratky plot (IQ^2 versus Q) of the same data. All curves exhibit a high-Q plateau, except that for the LOA−ZrO_2 case. Such a feature indicates the formation of Gaussian soft spheres.[31,32] This phenomena was also seen by Mackay et al[13] for tightly cross-linked PS nanoparticles. In our colloidal system, the clusters comprise an inorganic core and a grafted carboxylic acid. The density profile within the clusters is not uniform, thus leading to a plateau in the Kratky plot.

The Kratky plot for the LOA−ZrO_2 system, on the other hand, clearly reveals a single broad peak centered at Q = 0.04 Å^{-1} without the presence of a high-Q plateau. Such a peak was not seen in the SAXS data of the same sample when dispersed in hexane (Figure 2C). The Kratky plot for LOA−ZrO_2/chloroform is very similar to that observed for a hard sphere with a homogeneous density.[31] The most likely explanation is that LOA−ZrO_2 primary particles are homogeneously dispersed in chloroform without clustering.

Combining the SAXS and SANS data, we found that there are two types of dispersion behaviors for the same LOA−ZrO_2 sample. They exist as primary particles when dispersed in chloroform and as secondary clusters when dispersed in other solvents. This requires some reasoning. One possibility is that the conformation of the grafted linoleic acid may change in different solvents, thus affecting the dispersion state. Linoleic acid is an unsaturated fatty acid, comprising an 18-carbon chain with two double bonds. Such a long chain is expected to have diverse conformations in the solvent.

To probe the conformation of grafted linoleic acid in different solvents, additional SANS measurements were made on 10 wt % dispersions of LOA−ZrO_2 in toluene and benzene. These data were compared with those collected with chloroform as the solvent in Figure 4. All SANS curves in Figure 4A exhibit a common contribution from the scattering of the ZrO_2 core (at low-Q region) as well as that of the grafted linoleic acid (contributing to the broad hump at Q > 0.1 Å^{-1}). Again, the power-law intensity decay ($I \sim Q^{-D_f}$) gives the fractal exponent in the range of Q = 0.03−0.08 Å^{-1}. The exponent D_f was 2.86 with chloroform as the solvent, 2.74 with benzene, and 2.33 with toluene. This is to say that the LOA−ZrO_2 had a more compact structure in chloroform than in toluene or benzene. The exponential decay of the SANS intensity at a small Q range follows the Guinier approximation, as demonstrated in Figure 4B. The radius of gyration, inversely proportional to the slope, is much smaller in the chloroform case compared with that with toluene or benzene as the solvent. Note that the hydrodynamic diameter of LOA-grafted ZrO_2 dispersed in chloroform is also the smallest, identified by dynamic light scattering (DLS) (see the Supporting Information, Figure S4).

We now examine the high-Q region (Q > 0.1 Å^{-1}) in Figure 4A. Here, the scattering intensity reveals a broad hump that was absent in the SAXS profiles collected with toluene and benzene as solvents (see the Supporting Information, Figure S5).

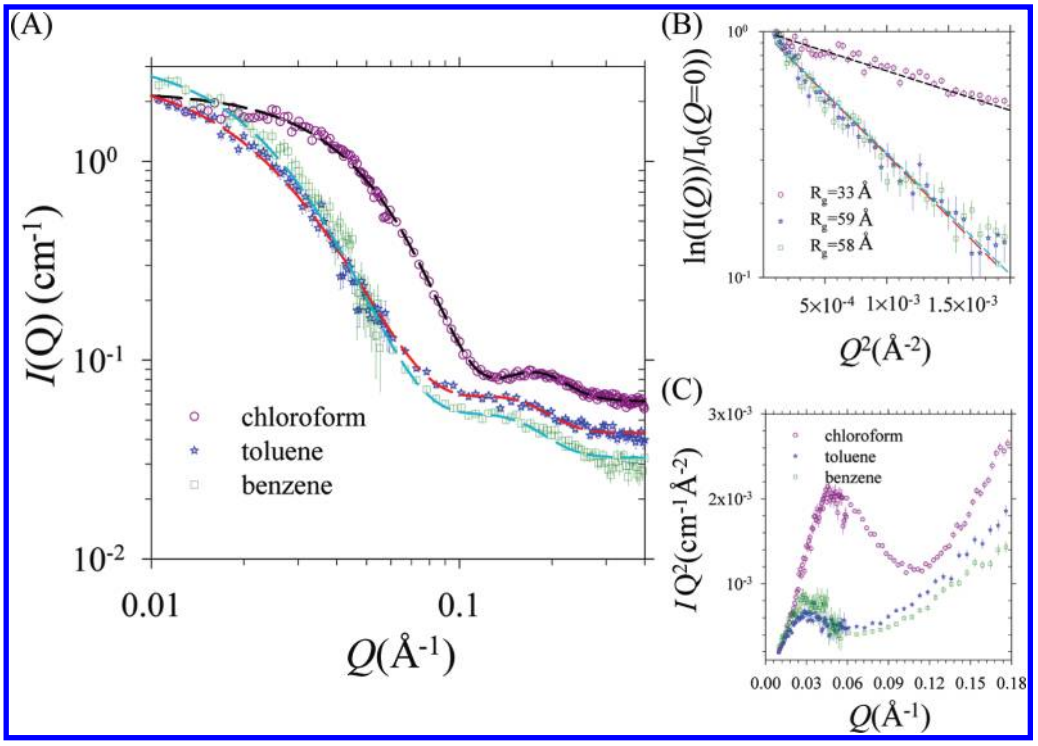

Figure 4. (A) Neutron scattering intensity data for LOA−ZrO_2 dispersed in chloroform, toluene, and benzene. Dashed curves were obtained by model fitting. Guinier plot (B) and Kratky plot (C) for the same SANS data set.

Table 3. Results of Fitting the LOA−ZrO_2 SANS Data with the Fractal Polydisperse Core−Shell Stucture Model

parameters	chloroform	toluene	benzene
block radius (Å)	12.4	10.5	12.1
fractal dimension	2.86	2.33	2.74
shell thickness (Å)	14.1	18.8	17.5
polydispersity	0.263	0.33	0.32
correlation length (Å)	14.1	42.7	35.1

The linoleic acid, containing only light elements, has an X-ray scattering length density of 8.52×10^{-6} Å^{-2}, similar to that of the solvent (toluene, 8.0×10^{-6} Å^{-2}; benzene, 8.02×10^{-6} Å^{-2}) and much smaller than that of ZrO_2 (4.31×10^{-5} Å^{-2}). Therefore, the X-ray is practically "blind" to the grafted linoleic acid against the solvent background. Comparatively, the neutron is much more sensitive. Thus, the extrabroad hump in the SANS profile reflects the local structure details of the organic shell.

Notice that a larger slope on the Guinier plot, or the radius of gyration, was observed when the same sample is dispersed in toluene or benzene then that in chloroform. This clearly indicates the clustering of particles in the first two solvents. To fit the SANS data, a fractal polydisperse core−shell model was implemented. During the fitting, the fractal dimension of the clusters was fixed to the values previously identified by a power-law analysis, that is, $D_f = 2.86$, 2.74, and 2.33 for cases with chloroform, benzene, and toluene, respectively. The neutron scattering length density of ZrO_2 was taken as $\rho^n_{ZrO_2} = 5.21 \times 10^{-6}$ Å^{-2}. That of solvents and linoleic acid were taken as $\rho^n_{chloroform} = 2.39 \times 10^{-6}$ Å^{-2}, $\rho^n_{toluene} = 9.4 \times 10^{-7}$ Å^{-2}, $\rho^n_{benzene} = 1.18 \times 10^{-6}$ Å^{-2}, and $\rho^n_{LOA} = 2.24 \times 10^{-7}$ Å^{-2}. The results have been plotted as dashed lines in Figure 4A to demonstrate the goodness of fit, whereas the structural parameters obtained are summarized in Table 3.

The clusters in toluene and benzene exhibit a blocking (core) raidus of 10.5−12 Å, with an organic shell of 17.5−18.8 Å in thickness and a correlation length of 35−43 Å. Although LOA-grafted ZrO_2 exists as loose, small clusters in C_6H_6, interpenetration of LOA chains among different LOA-grafted ZrO_2 in a cluster can be excluded. Furthermore, the cluster is 3 or 4 times the size of the primary particle. Therefore, each cluster only comprises several primary particles. Within a cluster, very little surface area of each primary particle is in contact with that of its neighbors. On average, for primary particles within the cluster, the shell composed of grafted LOA still exhibits a single monolayer thickness. The same LOA−ZrO_2 in chloroform has a blocking (core) radius similar to the other cases, but with a thinner shell and a much shorter correlation length. The correlation length is only 14.1 Å, comparable to the core size. This is a strong indication that the chloroform dispersion is made of primary particles with a compact core.

The fitting results can be best represented by the Kratky plot (Figure 4C) where a characteristic maximum for a particle-like dispersion[13,31,32] is observed. The larger and softer clusters formed in toluene or benzene produced a much weaker maximum and at a smaller Q value compared to that in chloroform. For the latter case, the upward trend at high Q is also sharper. This indicates the strong neutron scattering from more or less rigid entities at a very small scale. This must have come from the thinner and more compact conformation of the organic shell in chloroform than that in toluene or benzene.

The conformation of a solute is often related to the solubility parameter of the solvent. However, the solubility parameters for these three solvents [$\delta_{chloroform} = 9.3$, $\delta_{toluene} = 8.9$, and $\delta_{benzene} = 9.2$ (cal/cm^3)$^{1/2}$][33] are very similar, which cannot explain our

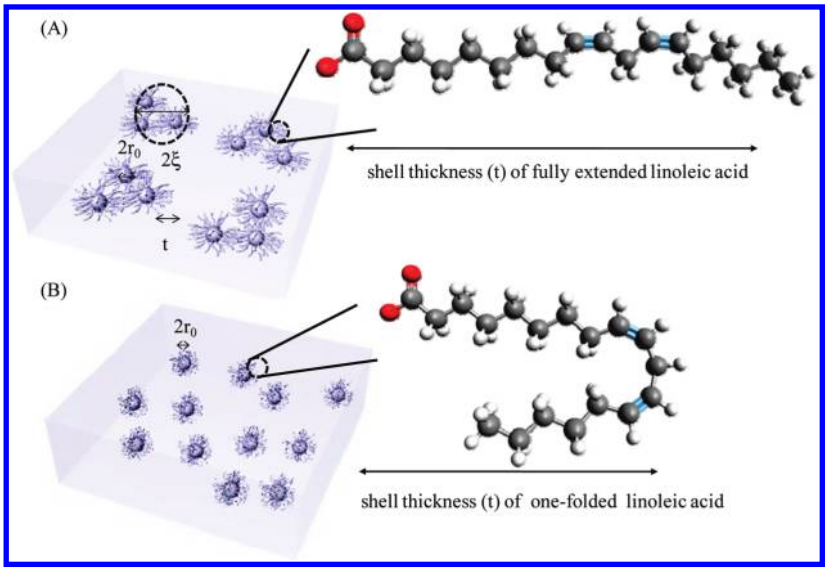

Figure 5. Schematic illustration of (A) the LOA−ZrO_2 clusters dipsersed in toluene and benzene. The grafted LOA chains are fully extended in both solvents. (B) The LOA−ZrO_2 primary particle dispersed in chloroform.

findings. A different proposition is thus needed to explain the shrinking of the shell thickness in chloroform.

Given that linoleic acid is an unsaturated fatty acid containing two cis double bonds, we speculate that these double bonds might interact with the aromatic ring of toluene and bezene. It would be easier for the aromatic solvent to swell and "interact" with the grafted linoleic acid, thus creating a brush conformation, as schematically illustrated in Figure 5. Without the intervention of solvent, the intrachain $\pi-\pi$ interaction of linoleic acid might induce a chain folding that leads to a thinner and more compact shell.

The interaction between LOA molecules with aromatic-ring-containing solvents was verified by liquid-state 500 MHz ^{1}H NMR measurements. Dispersions (10 wt %) of LOA−ZrO_2, as for the SANS measurements, and pure LOA were prepared in deteurated benzene (C_6D_6) and chloroform ($CDCl_3$). The ^{1}H NMR spectra of the dissolved LOA and LOA−ZrO_2 in these deuterated solvents are shown in Figure 6, where the signals are assigned according to the ^{1}H NMR decoupling experiments (see the Supporting Information, Figure S6).

Figure 6 revealed different chemical shifts for the dissolved LOA molecules in $CDCl_3$ (Figure 6A) and in C_6D_6 (Figure 6C). The differences are particularly obvious for the signals of CH_2 groups ($H_{a\&b}$) close to the carboxylic group and that of CH_2 groups ($H_{d\&g}$) in the vicinity of the alkene. The carboxylic group is an electron-withdrawing substituent. Therefore, the nucleus of CH_2 groups in the vicinity of the substituent is deshielded due to the reduced electron density. The electron-withdrawing ability of the carboxylic group is affected by its interaction with the solvent and is weaker in C_6D_6 than in $CDCl_3$. Consequently, the deshielding effect is weaker in C_6D_6 and the H_a and H_b appeared relatively upfield compared with that in $CDCl_3$.[34,35] On the other hand, the signals for H_{e-g} appeared approximately 0.1−0.135 ppm downfield in C_6D_6 than that in $CDCl_3$. The downfield shifts of H_{e-g} is most likely the result of the induced deshielding from the interaction of the double bonds with the more polarizable π eclectons of the C_6D_6 phenyl rings.

The ^{1}H NMR spectra (Figure 6B,D) of the LOA−ZrO_2 demonstrate the effects of anchoring LOA on ZrO_2. Particularly,

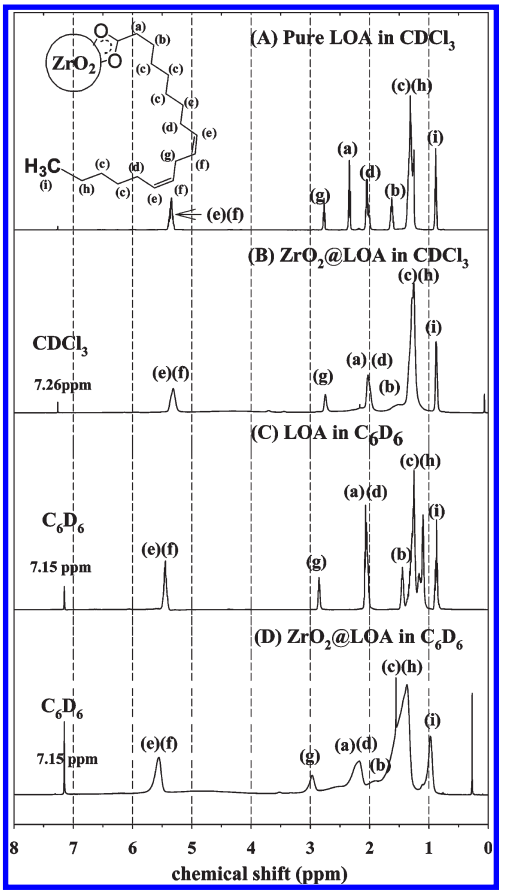

Figure 6. Proton NMR spectra of dissolved LOA and LOA−ZrO_2 in deuterated (A, B) chloroform and (C, D) benzene. The inset reveals the chemical structure with proton positions labeled.

the signals of Ha-b almost disappeared and turned into two extremely broad peaks. This arose from the dramatically reduced mobility of the grafted LOA.[36] The solvent influence is also present here, as all signals for the grafted LOA moved downfield

dx.doi.org/10.1021/jp202243z |J. Phys. Chem. C 2011, 115, 11941–11950

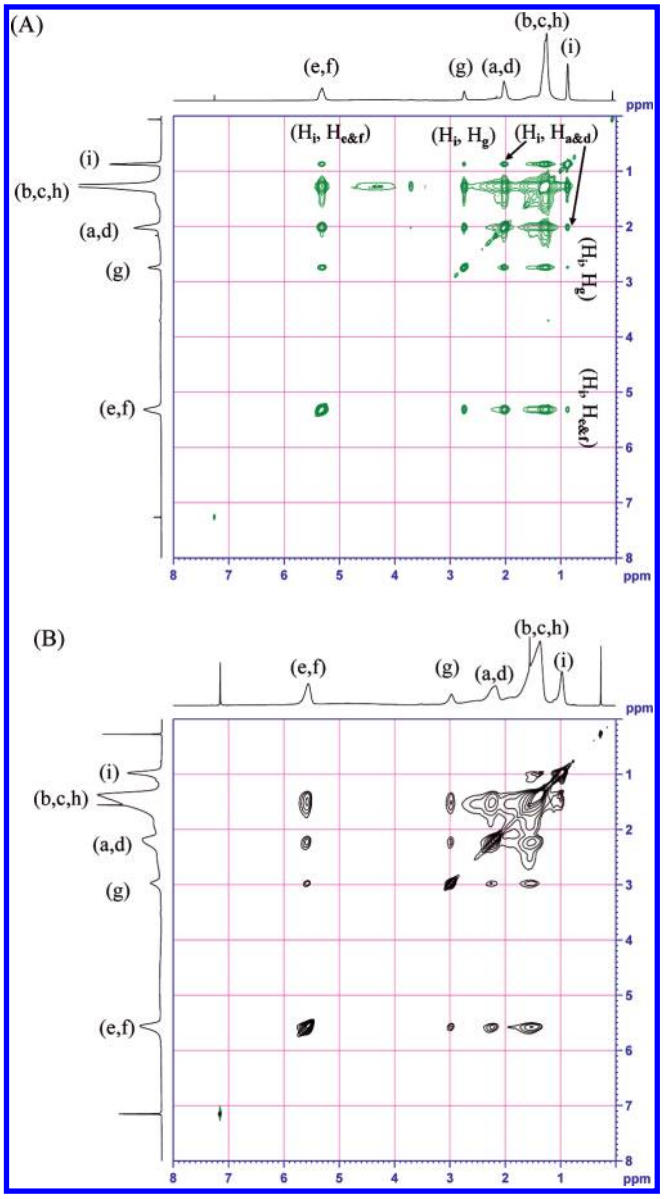

Figure 7. 2D NOESY spectra of LOA−ZrO_2 dispersed in deuterated (A) chloroform and (B) benzene.

in C_6D_6. Solvent is known to exert a strong influence on the cation−anion ion pair complexes, where the cation−anion interaction is stronger in less polar solvent (e.g., C_6D_6).[37] In C_6D_6, the ionic interaction between the carboxylic group with the ZrO_2 surface may be stronger and affects the whole LOA chain.

The organic shell structure of the LOA−ZrO_2 was further investigated by 2D NOESY NMR. Figure 7 shows the 2D NOESY spectra of LOA−ZrO_2 dispersed in $CDCl_3$ and C_6D_6. The spectrum displays diagonal peaks and crosspeaks. The latter correspond to pairs of protons that are near neighbor in space (<5 Å). The intensities of the crosspeaks decrease with the sixth power of the distance between the protons.[34] The crosspeaks between H_i−$H_{e\&f}$, H_i−H_g, and H_i−$H_{a\&d}$ pairs, which appear in the $CDCl_3$ case (Figure 7A), but not in the C_6D_6 case (Figure 7B), are particularly interesting. The absence or much weaker intensity of these crosspeaks in the C_6D_6 indicates that these pairs are separated by a longer distance in C_6D_6, as it should if the grafted chains are swollen by the solvent and stretch into a brushlike conformation. On the other hand, the proximity between H_i with $H_{a\&d}$ strongly suggests that the grafted LOA chains are folded in $CDCl_3$, which, therefore, confirms our interpretation based on the SANS results. However, the proposed folding of LOA on the particle surface might not be the only possible configuration that leads to an enhancement of H_i−H_g and H_i−$H_{e\&f}$ crosspeaks. The enhancement of these crosspeaks might be attributed to a lower intermolecular distance; namely, the swelling (expansion) and deswelling (collapse) of the shell by the solvent lead to a different orientation of the LOA molecules on the particle surface.[38] Alternatively a monolayer of LOA with their alkyl chains all tilted in the same direction might also lead to a thinner shell and shorten the distance between protons of different molecules. However, although this may be conceivable on a flat surface, such an orientation on the outer surface of a particle would be difficult to imagine. Further clarification will be carried out as future work.

CONCLUSION

The size distributions of dispersed nanoparticles are routinely characterized with TEM or DLS. However, TEM gives only the structural details in the dry form, which may be different from the situation in liquid. DLS probes the system in the dispersed state, but the result is affected by the proper assignment of the refractive indexes for the particles and the solvent. When inorganic nanoparticles are small and modified by organics, the latter may occupy an appreciable volume fraction, thus making the assignment of its refractive index difficult. The uncertainty in the refractive index leads to a rough estimation of the particle size. Only with the SAXS/SANS measurements is one able to obtain precisely the structural details of surface-modified nanoparticles, including the sizes of the inorganic core and the organic shell, as well as its secondary clusters.

The clustering and dispersion behavior of carboxylic acid-modified zirconia nanoparticles in different solvents as determined from SAXS/SANS measurements has been presented. In most cases, the transparent colloidal sol consists of "soft" secondary clusters generated from the nanoparticles. Only in one special condition, with linoleic acid modification and in chloroform, were the nanoparticles dispersed as primary units. The fact that the same entity appeared as secondary clusters in toluene and benzene, but as primary nanoparticles in chloroform, gave us an opportunity to understand the effect of solvent on the stabilization of the colloidal system.

The findings indicate that a colloidal system can be stabilized as either primary nanoparticles or aggregated clusters depending on the conformation of the grafting organic layer. The layer exhibits a swollen brush conformation when there are strong interactions between the grafted molecules and the solvent. Cluster dispersion is favored under such a circumstance. Conversely, a more compact organic layer is formed if the solvent does not swell the grafted molecules. The dispersion can then be stabilized as primary particles.

ASSOCIATED CONTENT

Supporting Information. FTIR spectra of carboxylic acid-modified ZrO_2 (Figure S1); TGA of carboxylic acid-modified ZrO_2 (Figure S2); UV/vis spectra of LOA-modified ZrO_2 in different solvents (Figure S3); size distributions of LOA−ZrO_2

dispersed in chloroform, benzene, and toluene measured by DLS (Figure S4); SAXS data and corresponding Kratky plot of LOA−ZrO_2 dispersed in benzene and toluene (Figure S5); and 1D NMR spectrum and decoupled spectra of LOA−ZrO_2 dispersed in $CDCl_3$ (Figure S6). This material is available free of charge via the Internet at http://pubs.acs.org.

AUTHOR INFORMATION

Corresponding Author

*E-mail: yssun@cc.ncu.edu.tw.

ACKNOWLEDGMENT

The National Science Council provided the financial support (NSC 98-2120-M-008-004-). We thank Dr. U-Ser Jeng, Dr. Chiu-Hun Su, and Dr. Chun-Jen Su for their assistance in the SAXS experiments at beamline BL23A in the NSRRC. We also thank Dr. Mai Anh Burke for her assistance during SANS measurements.

REFERENCES

(1) Garnweitner, G.; Goldenberg, L. M.; Sakhno, O. V.; Antonietti, M.; Niederberger, M.; Stumpe, J. Large-scale synthesis of organophilic zirconia nanoparticles and their application in organic-inorganic nanocomposites for efficient volume holography. *Small* **2007**, *3*, 1626–1632.

(2) Sakhno, O. V.; Goldenberg, L. M.; Stumpe, J.; Smirnova, T. N. Surface modified ZrO_2 and TiO_2 nanoparticles embedded in organic photopolymers for highly effective and UV-stable volume holograms. *Nanotechnology* **2007**, *18*, 105704.

(3) Suzuki, N.; Tomita, Y.; Ohmori, K.; Hidaka, M.; Chikama, K. Highly transparent ZrO_2 nanoparticle-dispersed acrylate photopolymers for volume holographic recording. *Opt. Express* **2006**, *14*, 12712–12719.

(4) Lee, S. K.; Shin, H. J.; Yoon, S. M.; Yi, D. K.; Choi, J. Y.; Paik, U. Refractive index engineering of transparent ZrO_2-polydimethylsiloxane nanocomposites. *J. Mater. Chem.* **2008**, *18*, 1751–1755.

(5) Otsuka, T.; Chujo, Y. Synthesis of transparent poly(vinylidene fluoride) (PVdF)/zirconium oxide hybrids without crystallization of PVdF chains. *Polymer* **2009**, *50*, 3174–3181.

(6) Hu, Y. Q.; Zhou, S. X.; Wu, L. M. Surface mechanical properties of transparent poly(methyl methacrylate)/zirconia nanocomposites prepared by in situ bulk polymerization. *Polymer* **2009**, *50*, 3609–3616.

(7) Imai, Y.; Terahara, A.; Hakuta, Y.; Matsui, K.; Hayashi, H.; Ueno, N. Transparent poly(bisphenol A carbonate)-based nanocomposites with high refractive index nanoparticles. *Eur. Polym. J.* **2009**, *45*, 630–638.

(8) Nakayama, N.; Hayashi, T. Synthesis of novel UV-curable difunctional thiourethane methacrylate and studies on organic-inorganic nanocomposite hard coatings for high refractive index plastic lenses. *Prog. Org. Coat.* **2008**, *62*, 274–284.

(9) Scholz, S.; Kaskel, S. Surface functionalization of ZrO_2 nanocrystallites for the integration into acrylate nanocomposite films. *J. Colloid Interface Sci.* **2008**, *323*, 84–91.

(10) Xu, K.; Zhou, S. X.; Wu, L. M. Dispersion of γ-methacryloxypropyltrimethoxysilane-functionalized zirconia nanoparticles in UV-curable formulations and properties of their cured coatings. *Prog. Org. Coat.* **2010**, *67*, 302–310.

(11) Akcora, P.; Liu, H.; Kumar, S. K.; Moll, J.; Li, Y.; Benicewicz, B. C.; Schadler, L. S.; Acehan, D.; Panagiotopoulos, A. Z.; Pryamitsyn, V.; Ganesan, V.; Ilavsky, J.; Thiyagarajan, P.; Colby, R. H.; Douglas, J. F. Anisotropic self-assembly of spherical polymer-grafted nanoparticles. *Nat. Mater.* **2009**, *8*, 354–359.

(12) Pryamtisyn, V.; Ganesan, V.; Panagiotopoulos, A. Z.; Liu, H. J.; Kumar, S. K. Modeling the anisotropic self-assembly of spherical polymer-grafted nanoparticles. *J. Chem. Phys.* **2009**, *131*, 221102.

(13) Mackay, M. E.; Dao, T. T.; Tuteja, A.; Ho, D. L.; Van Horn, B.; Kim, H. C.; Hawker, C. J. Nanoscale effects leading to non-Einstein-like decrease in viscosity. *Nat. Mater.* **2003**, *2*, 762–766.

(14) Acierno, D.; Filippone, G.; Romeo, G.; Russo, P. Dynamics of stress bearing particle networks in poly(propylene)/alumina nanohybrids. *Macromol. Mater. Eng.* **2007**, *292*, 347–353.

(15) Starr, F. W.; Douglas, J. F.; Glotzer, S. C. Origin of particle clustering in a simulated polymer nanocomposite and its impact on rheology. *J. Chem. Phys.* **2003**, *119*, 1777–1788.

(16) Crosby, A. J.; Lee, J. Y. Polymer nanocomposites: The "nano" effect on mechanical properties. *Polym. Rev.* **2007**, *47*, 217–229.

(17) Arita, T.; Yoo, J.; Ueda, Y.; Adschiri, T. Size and size distribution balance the dispersion of colloidal CeO_2 nanoparticles in organic solvents. *Nanoscale* **2010**, *2*, 689–693.

(18) Arita, T.; Ueda, Y.; Minami, K.; Naka, T.; Adschiri, T. Dispersion of fatty acid surface modified ceria nanocrystals in various organic solvents. *Ind. Eng. Chem. Res.* **2010**, *49*, 1947–1952.

(19) Luo, K. Q.; Zhou, S. X.; Wu, L. M.; Gu, G. X. Dispersion and functionalization of nonaqueous synthesized zirconia nanocrystals via attachment of silane coupling agents. *Langmuir* **2008**, *24*, 11497–11505.

(20) Zhou, S. X.; Garnweitner, G.; Niederberger, M.; Antonietti, M. Dispersion behavior of zirconia nanocrystals and their surface functionalization with vinyl group-containing ligands. *Langmuir* **2007**, *23*, 9178–9187.

(21) Chen, C. W.; Yang, X. S.; Chiang, A. S. T. An aqueous process for the production of fully dispersible t-ZrO_2 nanocrystals. *J. Taiwan Inst. Chem. Eng.* **2009**, *40*, 296–301.

(22) Jeng, U. S.; Su, C. H.; Su, C. J.; Liao, K. F.; Chuang, W. T.; Lai, Y. H.; Chang, J. W.; Chen, Y. J.; Huang, Y. S.; Lee, M. T.; Yu, K. L.; Lin, J. M.; Liu, D. G.; Chang, C. F.; Liu, C. Y.; Chang, C. H.; Liang, K. S. A small/wide-angle X-ray scattering instrument for structural characterization of air-liquid interfaces, thin films and bulk specimens. *J. Appl. Crystallogr.* **2010**, *43*, 110–121.

(23) Gilbert, E. P.; Schulz, J. C.; Noakes, T. J. "Quokka" - the small-angle neutron scattering instrument at OPAL. *Physica B* **2006**, *385−86*, 1180–1182.

(24) Kline, S. R. Reduction and analysis of SANS and USANS data using IGOR Pro. *J. Appl. Crystallogr.* **2006**, *39*, 895–900.

(25) Beaucage, G. Approximations leading to a unified exponential power-law approach to small-angle scattering. *J. Appl. Crystallogr.* **1995**, *28*, 717–728.

(26) Roe, R. J. *Methods of X-ray and Neutron Scattering in Polymer Science*; Oxford University Press: New York, 2000; Chapter 5, p 155.

(27) Bartlett, P.; Ottewill, R. H. A neutron-scattering study of the structure of a bimodal colloidal crystal. *J. Chem. Phys.* **1992**, *96*, 3306–3318.

(28) Lin, J. M.; Lin, T. L.; Jeng, U. S.; Zhong, Y. J.; Yeh, C. T.; Chen, T. Y. Fractal aggregates of the Pt nanoparticles synthesized by the polyol process and poly(*N*-vinyl-2-pyrrolidone) reduction. *J. Appl. Crystallogr.* **2007**, *40*, S540–S543.

(29) Teixeira, J. Small-angle scattering by fractal systems. *J. Appl. Crystallogr.* **1988**, *21*, 781–785.

(30) Kolb, M.; Botet, R.; Jullien, R. Scaling of kinetically growing clusters. *Phys. Rev. Lett.* **1983**, *51*, 1123–1126.

(31) Burchard, W.; Kajiwara, K.; Nerger, D. Static and dynamic scattering behavior of regularly branched chains: A model of soft-sphere microgels. *J. Polym. Sci., Polym. Phys. Ed.* **1982**, *20*, 157–171.

(32) Tuteja, A.; Duxbury, P. M.; Mackay, M. E. Polymer chain swelling induced by dispersed nanoparticles. *Phys. Rev. Lett.* **2008**, *100*, 077801.

(33) Barton, A. F. M. Solubility parameters. *Chem. Rev.* **1975**, *75*, 731–753.

(34) Jacobsen, N. E. *NMR Spectroscopy Explained*; John Wiley & Sons, Inc.: Hoboken, NJ, 2007; Chapters 2 and 10, pp 39−73 and 408−488.

(35) Williams, D. H.; Bhacca, N. S. Solvent effect in NMR spectroscopy-III chemical shifts induced by benzene in ketones. *Tetrahedron* **1965**, *21*, 2021–2028.

(36) Kim, T. H.; Choi, S. M.; Kline, S. R. Polymerized rodlike nanoparticles with controlled surface charge density. *Langmuir* **2006**, *22*, 2844–2850.

(37) Chen, M. C.; Robert, J. A. S.; Marks, T. J. Marked counteranion effects on single-site olefin polymerization processes. Correlations of ion pair structure and dynamics with polymerization activity, chain transfer, and syndioselectivity. *J. Am. Chem. Soc.* **2004**, *126*, 4605–4625.

(38) Von, W. G.; Kitchens, C. L. Small-angle neutron scattering of silver nanoparticles in gas-expanded hexane. *J. Phys. Chem. C* **2010**, *114*, 16285–16291.